Advances in Computational Design, *Vol. 8, No. 3 (2023) 191-217*
https://doi.org/10.12989/acd.2023.8.3.191

Design and analysis of offshore wind structure

Young-Suk You[1], Min-Young Sun**[1] and Young-Ho Lee*[2]

[1]*JBNU International Offshore Wind International Research Institute, Department of EnergyMechanical Design Engineering, Jeonbuk National University, 567 Baekje-daero, Jeonju, Republic of Korea*
[2]*Department of Mechanical Engineering, Korea Maritime and Ocean University, 727 Taejong-ro, Busan, Republic of Korea*

(Received August 19, 2020, Revised November 2, 2021, Accepted October 20, 2022)

Abstract. The objective of this study was to evaluate the foundation structure of a 3.6-MW wind turbine generator (WTG) installed offshore in Western Korea. The ultimate limit state (ULS) and fatigue limit state (FLS) of the multi-pile steel foundation (MSF) installed at the Saemangeum offshore wind farm were structurally investigated using the finite element (FE) software, ANSYS Workbench 19.0. According to the ULS analysis, no plastic deformation was found in any of the components constituting the substructure. At the same time, the maximal stress value reached the calculation limit of 335 MPa. According to the FLS results, the stress concentration factor (SCF) ranged from 1.00 to 1.88 in all components. The results of this study can be applied to determine the optimal design for MSFs.

Keywords: fatigue limit state; finite element method; multi-pile steel foundation; SMG offshore wind farm; ultimate limit state;

1. Introduction

Today, the world's main energy source is fossil fuel. However, the volume of fossil fuels is limited, and their use contributes to environmental issues, such as air pollution and global warming. Offshore wind energy is a non-destructive renewable energy that has gained significant attention worldwide as an alternative reliable energy source. Various studies have been conducted worldwide on the supporting foundation for wind turbine. Svensson (2010) demonstrated that the differential settlements of several onshore foundations were significantly high, resulting in horizontal displacement of the tower tops by 155 mm. Devaney (2012) performed a stress analysis of the wave effect of the jacket structures supporting offshore wind turbines using a finite element method (FEM).

Seismic analysis is important not only in wind turbine structure, but also in general structures such as high building, tower crane and seismic analysis methods suitable for the characteristics of each structure must be performed (Gholipour *et al*. (2018), Ushio *et al*. (2019)). Mo *et al*. (2017) conducted a seismic fragility analysis of monopile offshore wind turbines under different operational conditions. According to their results, the seismic response of monopile wind turbines greatly affected by the frequency component of the ground motion records input. Further, Bogdán

*Corresponding author, Professor, E-mail: lyh@kmou.ac.kr
**Corresponding author, Professor, E-mail: smy5439@jbnu.ac.kr

http://www.techno-press.org/?journal=acd&subpage=7 ISSN: 2383-8477 (Print), 2466-0523 (Online)

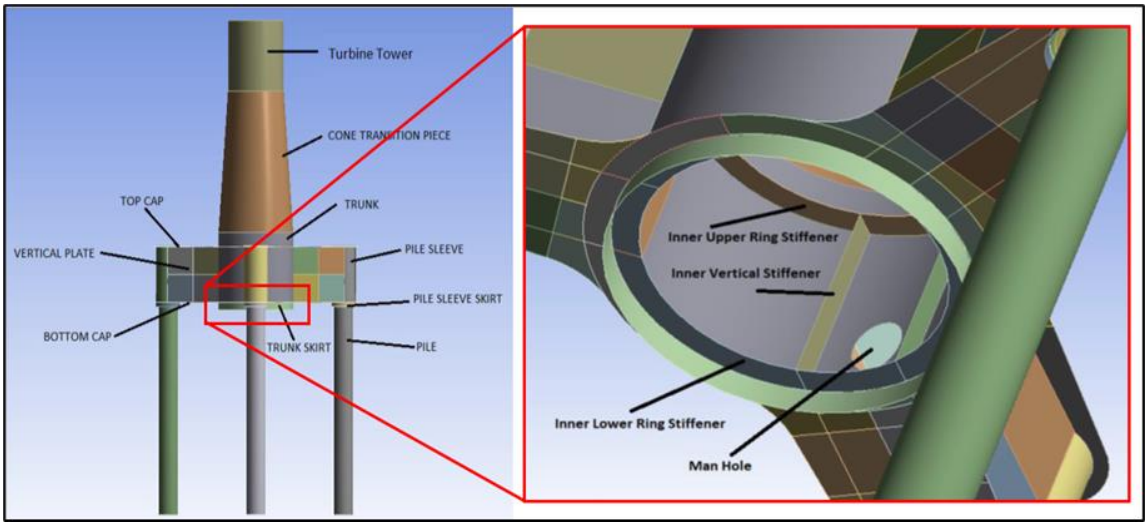

Fig. 1 Name of each part of the MSF

(2017) numerically modeled the foundations of offshore wind turbines. The results of the modeling revealed that the response of the foundations depends significantly on the relative density and vertical load rate of the soil. Ashish and Selvam (2013) also found that the effects of the vertical load rate and aspect ratio become more significant in dense soils. Chew *et al*. (2014) three- and four-legged foundation designs and concluded that three-legged jacket substructures are the most cost-efficient in transitional water depth, as they reduce required structural mass by approximately 17% and the number of welded joints by 25%. Kelma *et al*. (2015) conducted a probabilistic fatigue analysis of jacket support structures for offshore wind turbines exemplified on tubular joints and found that very high stress ranges are particularly significant for the determination of fatigue damage. Brandt *et al*. (2017) also conducted a numerical fatigue life evaluation using a meta-model approach, while Chen *et al*. (2016) predicted the mean maximum fatigue damage behavior of jackets using four out of seven available input parameters. Moreover, they performed a numerical global buckling analysis for all structures after validation with scaled-down experiments. According to their results, the proposed structures demonstrate excellent structural behavior and have few structural nodes or components. This makes them competitive with the patented twisted jacket structures, while they require the use of relatively few materials, similar to three-legged jacket structures. Yeter *et al*. (2016) evaluated the fatigue damage prediction of several spectral fatigue damage models, including Rayleigh, Wirsching-Light, Tunna, α0.75, Tovo and Benasciutti, Zhao–Baker, Rice and Dirlik models. The sensitivity of the natural frequency of the support structure to variations in the pile foundation models of mono-towers, tripods, and lattice towers was investigated by Zaaijer (2002). The results demonstrated that a stiffness matrix with coupled lateral behavior has far fewer degrees of freedom than a comprehensive finite element (FE) model and therefore reduces the number of computations required in dynamic analysis. In this study, the multi-pile steel foundation (MSF) installed at the Saemangeum (SMG) offshore wind farm was analyzed to investigate its mechanical behavior using the ultimate limit state (ULS) and fatigue limit state (FLS). It is a lagoon surrounded by a seawall, and the water level is managed through a drainage lock gate.

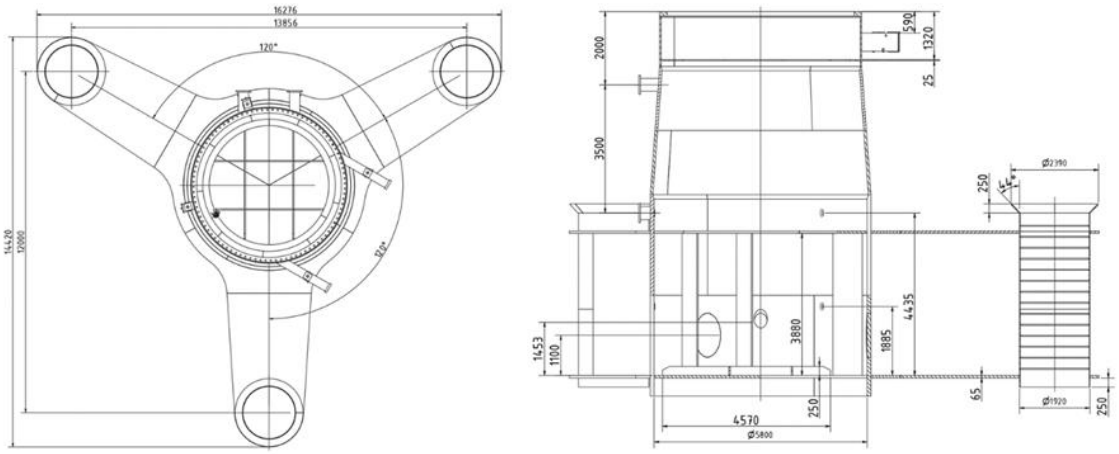

(a) (b)

Fig. 2 Dimensions of each part of the MSF (a) top view, (b) front view

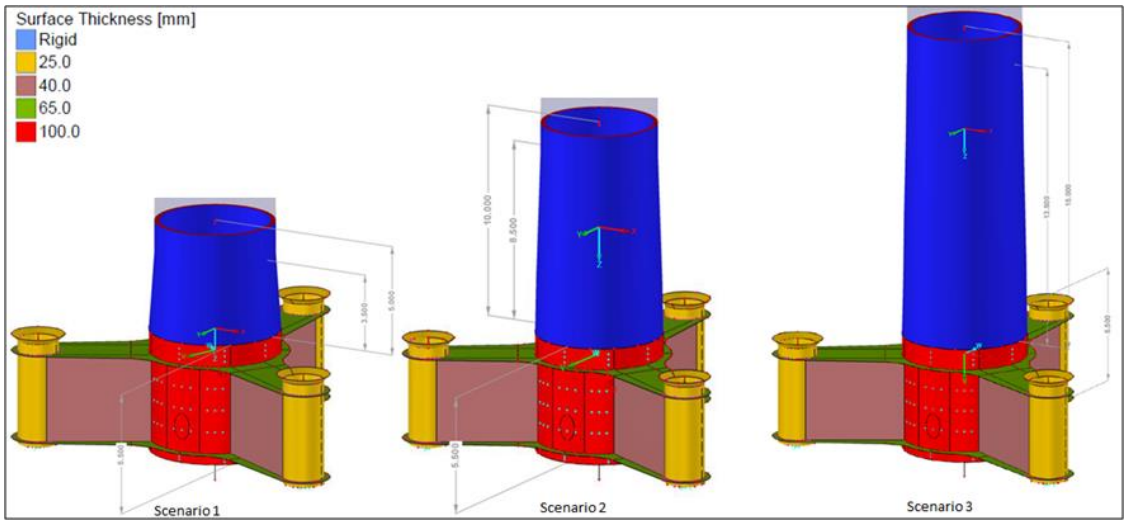

Fig. 3 Plate thicknesses of each scenario

2. Materials and methods

2.1 Finite-Element Model

2.1.1 Geometry

The foundation structure was created in the CAD construction software, Autodesk Inventor, and then imported into the FE software, ANSYS Workbench 19.0. Thus, the FE model represents the latest governing geometry. Based on DIN EN 1993-1-8:2010-12 (Eurocode 3), the investigation was conducted using a three-dimensional (3D) shell model considering the middle plane of the steel plates. The plate thicknesses and the detailed geometry of the foundation

Table 1 Material definition

Thickness [mm]	Plastic Strain [%]		
	0.0%	2.5%	40%
16-40	345 MPa	345 MPa	470 MPa
40-63	335 MPa	335 MPa	470 MPa
63-80	325 MPa	325 MPa	470 MPa
80-100	315 MPa	315 MPa	470 MPa
100-150	295 MPa	295 MPa	450 MPa

Table 2 S355 material thickness dependent nominal yield strength f_y and ultimate tensile strength f_u

Thickness [mm]	$16 < t \leq 40$		$40 < t \leq 63$		$63 < t \leq 80$		$80 < t \leq 100$		$100 < t \leq 150$	
	f_y	f_u	f_y	f_u	f_y	f_u	f_y	f_u	f_y	f_u
S355	345	470	335	470	325	470	315	470	295	470

structure are presented in Fig. 1-3. The geometry of the foundation was considered under three different scenarios (Scenarios 1–3) owing to the water depths of 5.0 m, 10.0 m, 15.0 m for each Scenarios (the interface between tower and foundation structure is at 5.0 m above the sea level) and the unfavorable stress distribution at the junction between the cone and cylindrical part of the central tube.

2.1.2 Material assignment

According to DIN EN 1993-1-8, DNVGL-RP-C205, and DNVGL-ST-0126, an elastoplastic material formulation with multi-linear kinematic isotropic hardening is considered for the ULS stress capability investigation in offshore steel structure. The following material parameters are considered based on DIN EN 1993-1-1: Young's modulus E of 210000 MPa, a Poisson ratio of 0.3, density of 7850 kg/m³, shear modulus G of 81000 N/mm and the coefficient of thermal expansion α of 12×10^{-6} per K.

The yield plateau with a constant stress above the yield limit has a length of 2.5%. This value is conservative since no hardening occurs and the yield plateau might be a little shorter in reality. When a strain of 2.5% is reached, the end of the plateau occurs and the stress increases from yield stress to ultimate stress assumed to happen at a plastic strain of 40%. This ultimate-strain value is conservative since the absorbed energy is equal to the area under the work curve and a high ultimate strain gives a smaller area. Since different plate thicknesses are used, the yield stress varies. S355 steel grade is chosen as a construction material, as it is the most common steel grade applied for substructure tubular fabrication. Under the DIN EN-10025(2005) material steel code and S. Maier (2015), the yield stress reduces with increased plate thicknesses. The yield and ultimate stresses for the different plate thicknesses based on DIN EN 10025 are listed in Table 1-2.

2.1.3 Mesh

The model had a meshed geometry with quadratic eight-node shell elements with six degrees of freedom at each node. A high element quality was obtained with an element aspect ratio of less than 3 in the area of interest. The model was meshed with a mesh size of 60 mm for the ULS

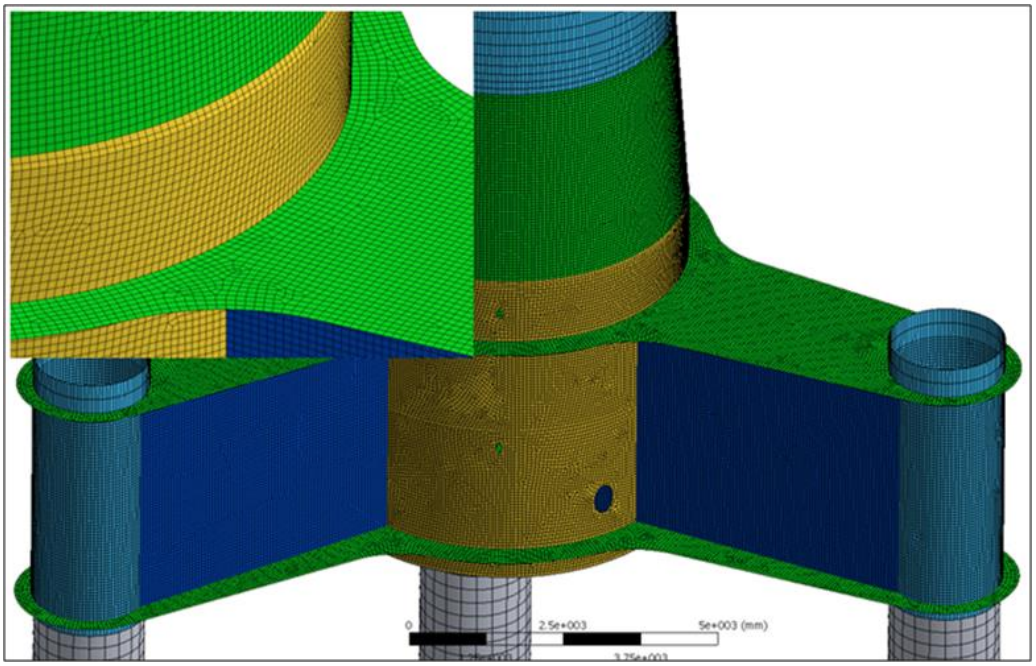

Fig. 4 Mesh for ULS

investigations and with a mesh size of 30 mm for the FLS investigations. These two meshes are presented in Figs. 4 and 5, respectively.

2.1.4 Applied boundary conditions

The piles were supported at the bottom so that all translational degrees of freedom could be achieved, while complete rotational freedom was also achieved. The pile-to-pile sleeve connection was realized with bonded contact elements between the pile top and the sleeve bottom. Because the simplification excluded a grouted connection, it was unreasonable to conduct an exact evaluation of the sleeves; this was done in a separate detailed design. A conservative assumption was made that no lateral constraints affected the pile height.

Ultimate Limit State

The maximum loads of the turbine have been released by the turbine manufacturer along with the 50-yr maximum wave, storm, wind, and current loads (Arany *et al*. 2016). First, the maximum loads on the foundations (predominantly overturning moment, lateral load, and vertical load) due to all possible design load cases were estimated and compared with the capacity of the chosen foundation (MSF-type). The ULS design provided the minimal dimensions (length and diameter) of the MSF and the required wall thickness. The necessary inputs for the calculations were the site characteristics (e.g., wind and wave data) and the turbine data. The load results are listed in Table 3. The four presented load cases listed in Table 3 were investigated by finite element analysis (FEA) in both the positive and negative directions. The loading was applied at a height of 20.0 m as forces (Figs. 6–9 (a)) and bending moments (Figs. 6–9 (b)) distributed over the top face of the cylindrical part of the central tube (only the positive direction is presented). The 20.0 m height for

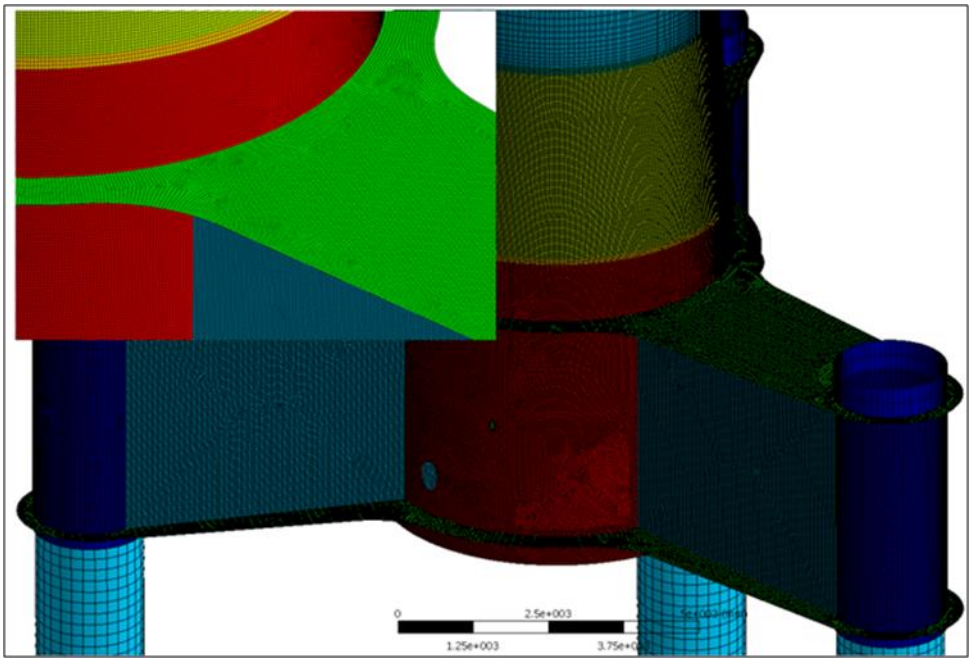

Fig. 5 Mesh for FLS

Table 3 Considered load cases for ULS

$1.35F_{res}$+$1.35F_z$+$1.35M_{res}$+$1.35M_z$+1.35Wave+1.35HydrostaticPressure								
Load Combination	F_x [kN]	F_y [kN]	F_{res} [kN]	F_z [kN]	M_x [kNm]	M_y [kNm]	M_{res} [kNm]	M_z [kNm]
LC 1	71.0	861.8	864.72	4495.4	83557.0	3318.4	83622.87	2182.6
LC 2	12.4	848.3	848.39	4462.0	83833.0	6033.1	84049.81	1723.7
LC 3	301.2	48.4	305.06	4149.6	5815.1	21688.4	22454.44	1613.7
LC 4	228.3	861.8	891.53	4495.4	83557.0	3318.4	83622.87	2182.6

the load application corresponds to the interface level in Scenario 3. Therefore, the analysis of the Scenario 1 structure is also applicable to the designs in Scenarios 2 and 3.

The wave loads were considered based on the ULS design shown in Fig. 10 (a), and the waves were conservatively applied in the same direction as the wind. A load of 810 kN attracted by the shaft was applied to the 0.0 m managed sea level (MSL). Loads of 270 kN attracted by the casing were applied to the tops of the pile sleeves, and a partial safety factor of 1.35 was considered for the loads. For the ULS design, the maximum water pressure on the closed casing was also taken into account. The maximum wave crest was considered to be +4.0 m from the MSL and the mudline to be –15.0 m from the MSL, with the resulting maximal water level difference being 19.0 m. According to DNVGL-OS-C101 (2016), the design value of the water pressure was calculated as follows using the partial safety factor for the loads ($\gamma = 1.35$):

$$P_h = 1.35 \cdot 19.0\, m \cdot 1.025\ t/m^3 \cdot 9.81\, m/s^2 = 258\, kN/m^2 \quad (1)$$

The overpressure was applied to the FE model as shown in Fig. 10 (b).

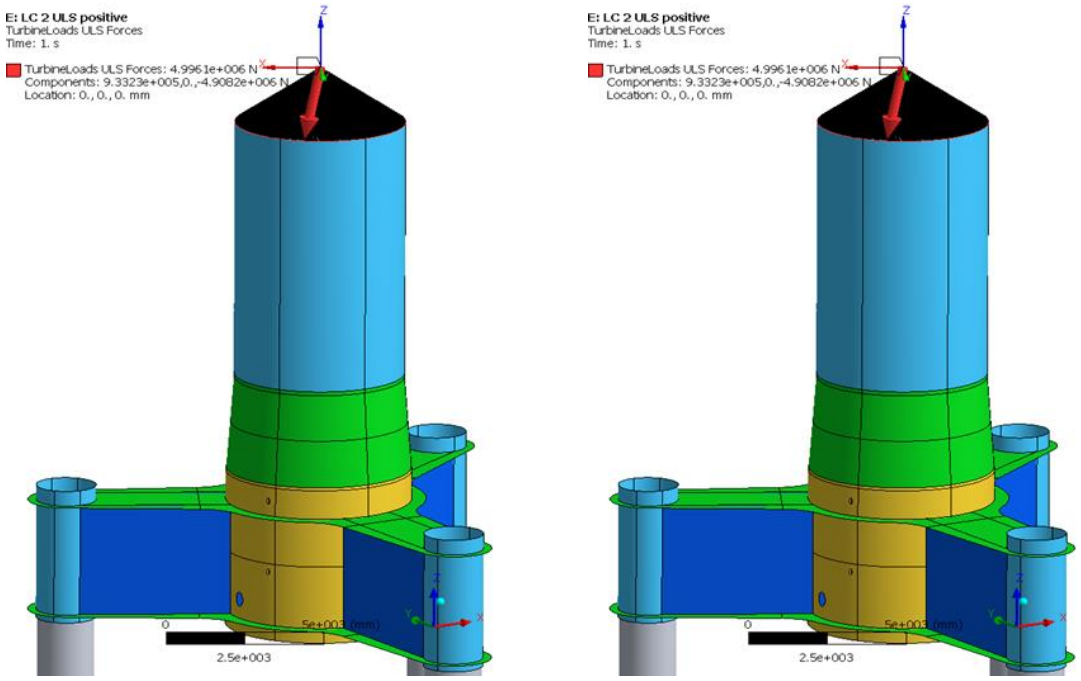

(a) (b)

Fig. 7 Considered LC 2 (a) ULS forces, (b) ULS moments

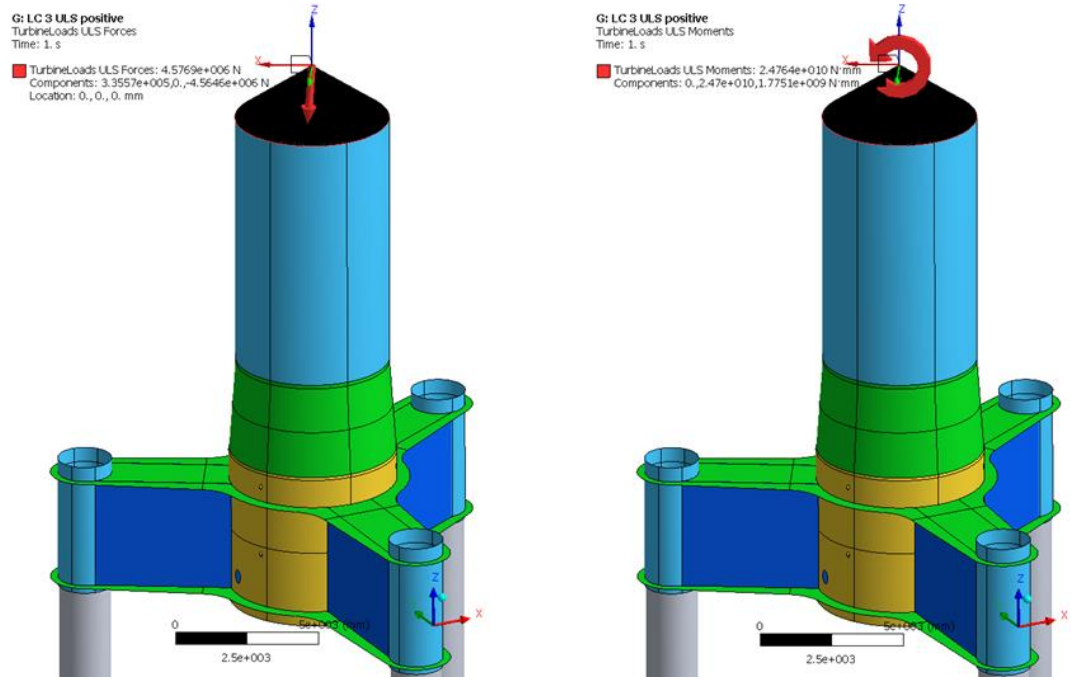

(a) (b)

Fig. 8 Considered LC 3 (a) ULS forces, (b) ULS moments

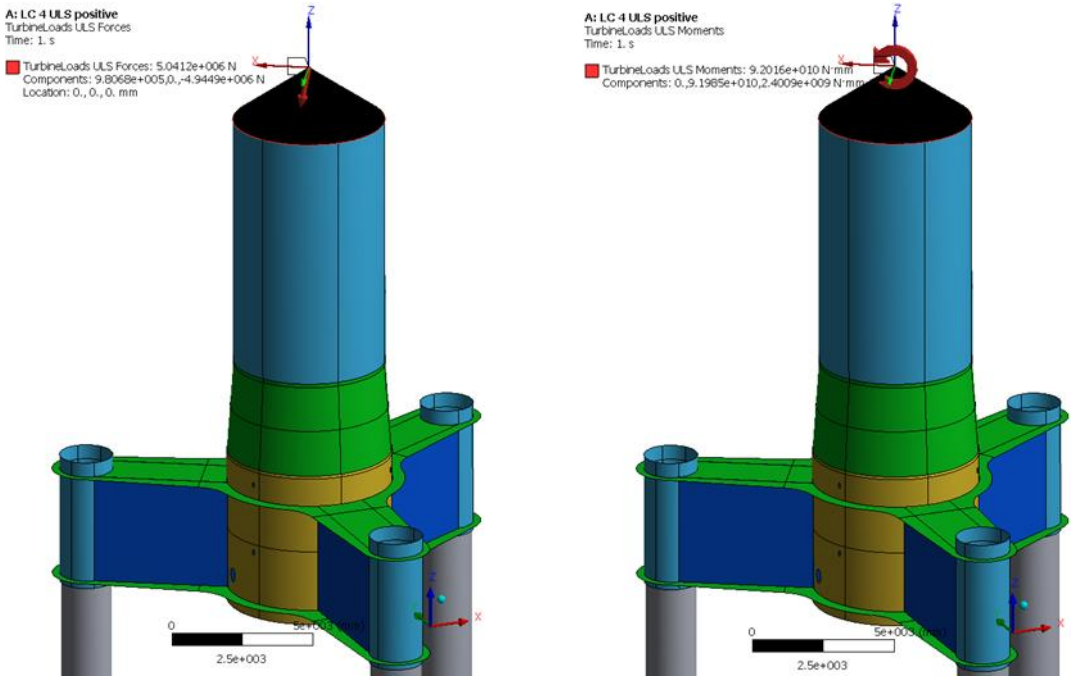

(a) (b)

Fig. 9 Considered LC 4 (a) ULS forces, (b) ULS moments

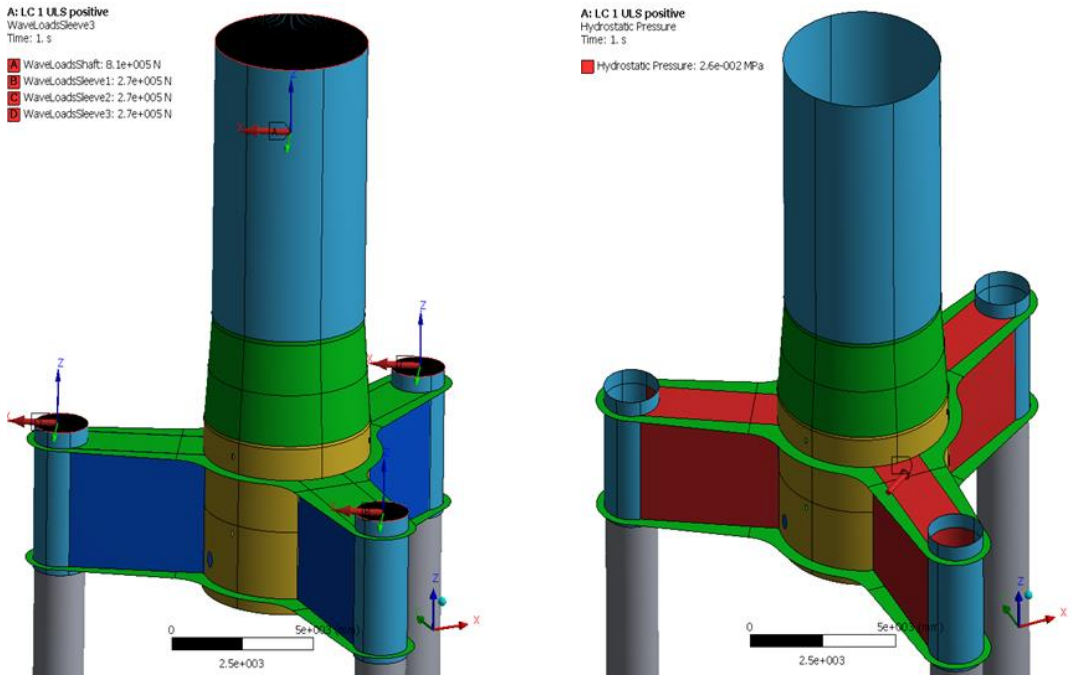

(a) (b)

Fig. 10 Applied wave load and water pressure (a) Wave loads, (b) Hydrostatic pressure

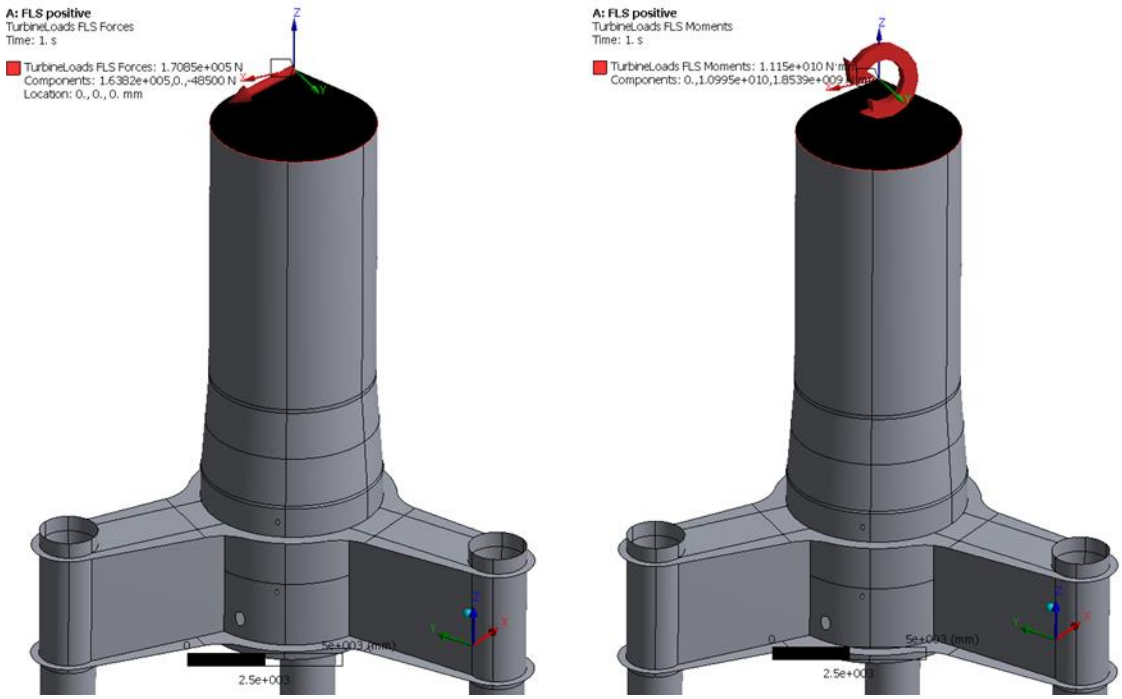

(a) (b)

Fig. 11 Considered DEL (a) FLS forces, (b) FLS Moments

Table 4 Considered DEL for FLS

Load Combination	F_x [kN]	F_y [kN]	F_{res} [kN]	F_z [kN]	M_x [kNm]	M_y [kNm]	M_{res} [kNm]	M_z [kNm]
FLS	141.30	82.90	163.82	48.50	5816.40	9330.30	10994.77	1853.90

Fatigue Limit State (FLS)

The FLS load acting on the foundation was realized as the damage equivalent load (DEL) for 2.00E8 cycles and m = 4. The load combination listed in Table 4 was investigated with the FE model in both the positive and negative directions. The load was applied at a height of 20.0 m in the form of forces (Fig. 11 (a)) and bending moments (Fig. 11 (b)) distributed over the top face of the cylindrical part of the central tube (only the positive direction is presented).

3. Results and discussions

3.1 Ultimate limit state verification

3.1.1 Stress capability verification of ultimate limit state

Load case 4 was dominant and is therefore documented in detail below. The FE analysis was evaluated with respect to deformations and stresses of the structure. The considered structure was composed of steel grade S355. Based on Gerven (2011), the thickness-dependent design yield

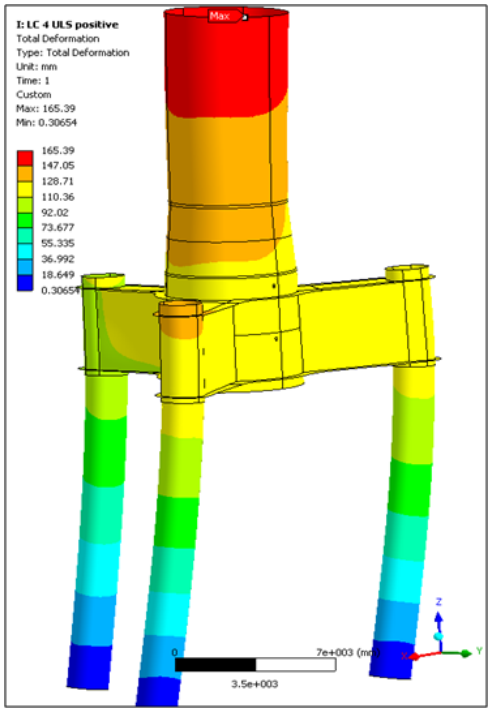

Fig. 12 Deformation of foundation structure;magnification factor of 20

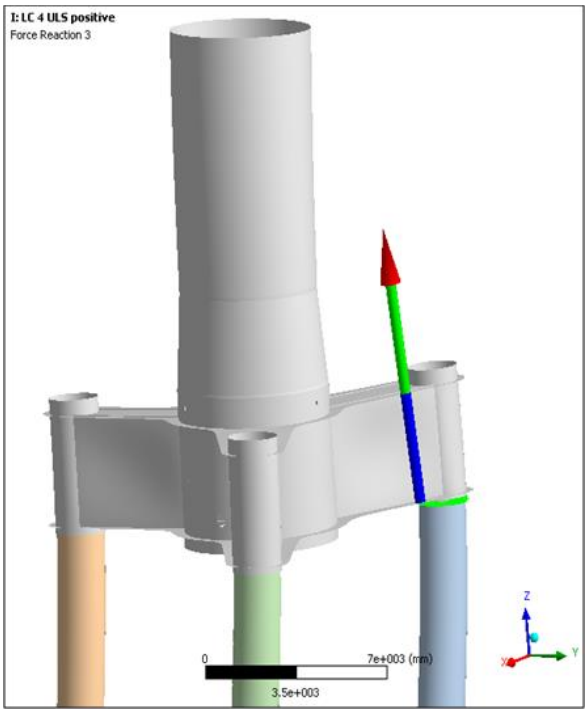

Fig. 13 Maximal reaction forces at pile top; magnification factor of 20

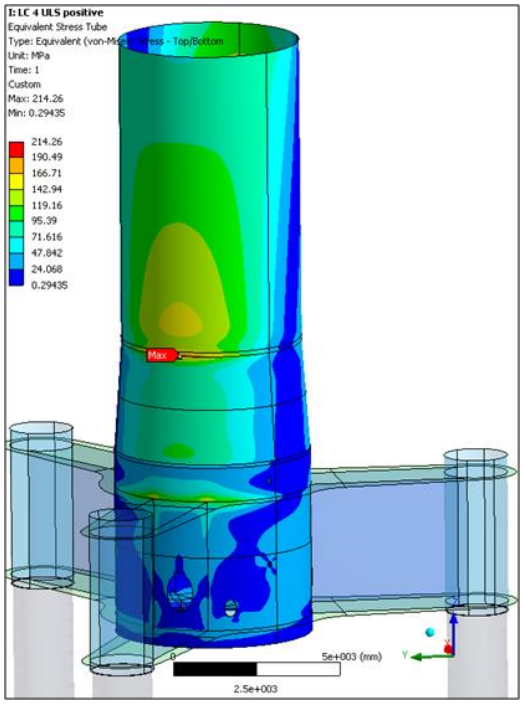

Fig. 14 Von Mises stresses at central tube

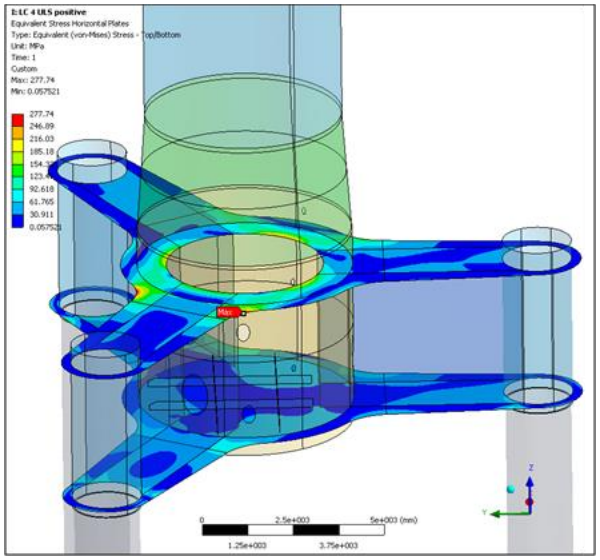

Fig. 15 Von Mises stresses and plastic strain at outer ring stiffener

strengths for steel grade S355 were chosen, with the material safety factor being γ_{M0} is 1.00 based on Maier (2015).

To evaluate the accuracy of the computed results, the deformations of the foundation structure (Fig. 12) as well as the maximal reaction forces at the pile top (Fig. 13) are shown. The FE model

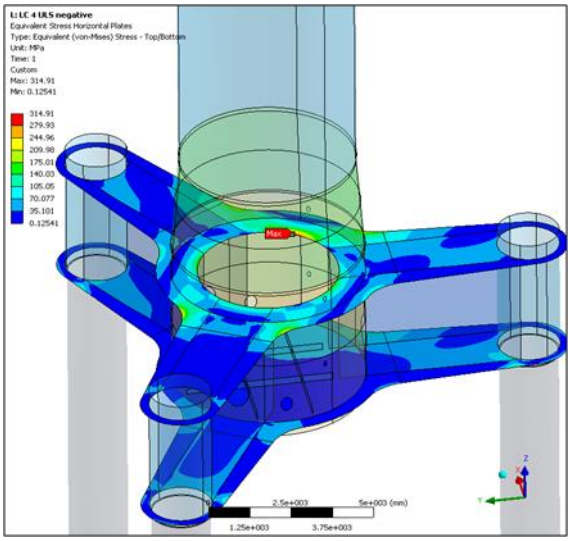

Fig. 16 Von Mises stresses at inner ring stiffener

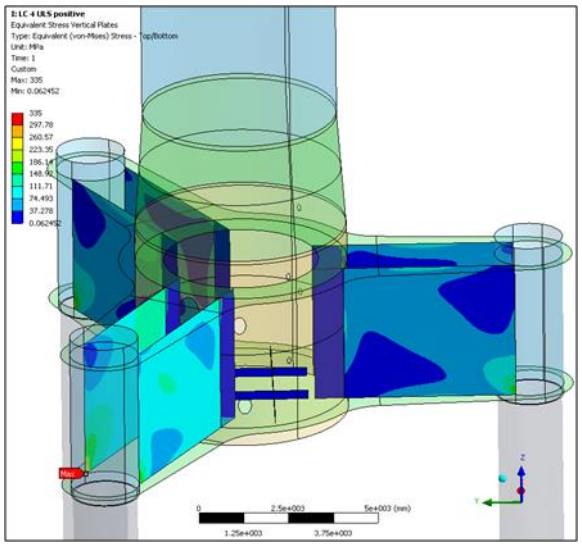

Fig. 17 Von Mises stresses at vertical plate

behaved as expected, and its functionality was confirmed. Figs. 14 present the von Mises stress and plastic strain distributions in the central tube, with the maximal value of 214 MPa being below the design yield stress limit of 325 MPa and translating to a plastic strain of 0.0%. Figs. 15–16 show the von Mises stress distribution in the horizontal plates, with the maximal values of 278 MPa at the outer ring stiffener and 315 MPa at the inner ring stiffener being below the yield strength limit of 325 MPa. Accordingly, no plastic strain was found to occur in the horizontal plates. The von Mises stress distribution in the vertical plates is presented in Fig. 17. It can be seen that the maximal stress value in this case reached the design yield stress limit of 335 MPa. The plastic strain at the edge of the connection to the sleeves was irrelevant, its value being 0.0% and

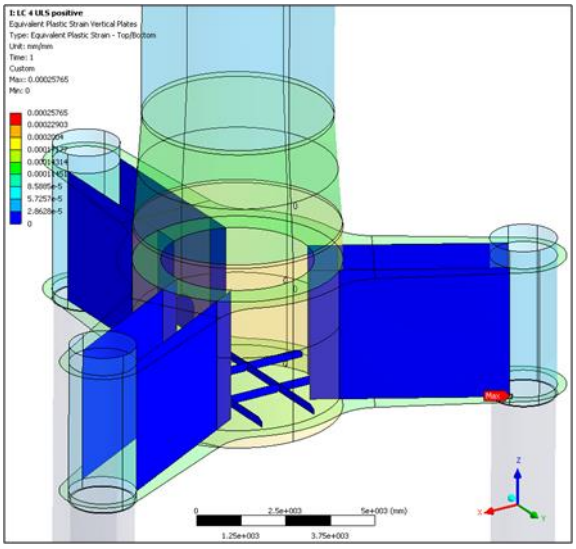

Fig. 18 Plastic strain at vertical plate

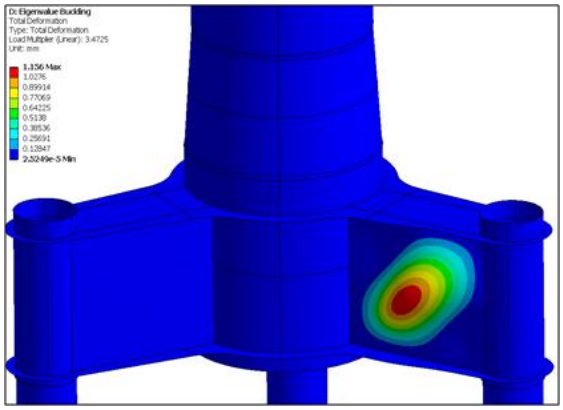

Fig. 19 First local mode at vertical plate

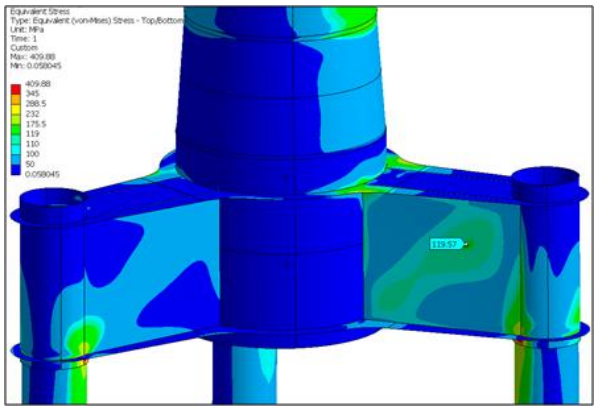

Fig. 20 Local von Mises stresses at vertical plate

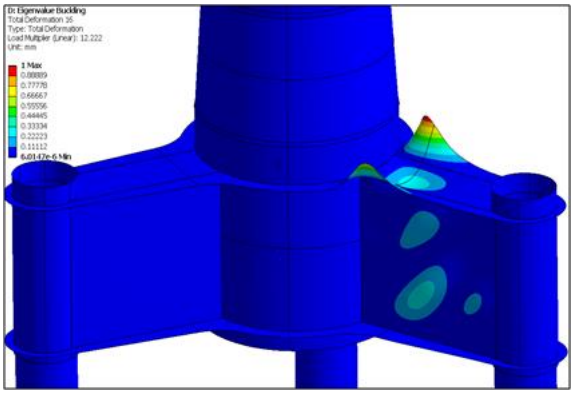

Fig. 21 First local mode at outer ring stiffener

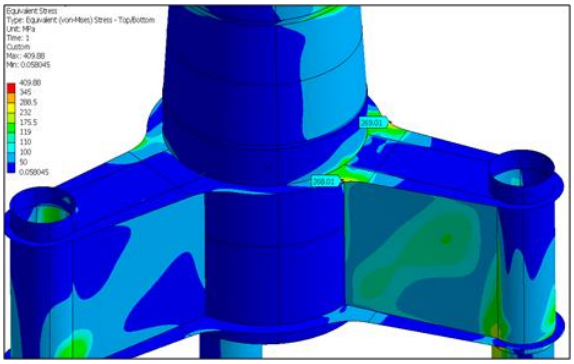

Fig. 22 Local von Mises stresses at outer ring stiffener

Table 5 Buckling-capability evaluation of vertical plate

Load case	LC4	Value	Unit
Location of buckling	Ring Stiffener		
Load factor (numerical)	kg	3.4725	[-]
Stress at buckling area	σ_{Rep}	120	[MPa]
Critical buckling stress	σ_{ki}	416.7	[MPa]
Yield strength	f_y	345	[MPa]
Reduced slenderness	Λ	0.910	[-]
Factor from buckling curve	k	0.833	[-]
Partial safety factor	γ_M	1.15	[-]
Buckling resistance	R_d	249.99	[MPa]
Load factor with imperfection	$R_d/\sigma_{\mathrm{Rep}}$	2.083	Proven
Check	$\sigma_{\mathrm{Rep}}/R_d$	0.480	Proven

Table 6 Buckling-capability evaluation of outer ring stiffener

Load case	LC4	Value	Unit
Location of buckling	Ring Stiffener		

Load factor(numerical)	kg	12.222	[-]
Stress at buckling area	σ_{Rep}	270	[MPa]
Critical buckling stress	σ_{ki}	3299.94	[MPa]
Yield strength	f_y	325	[MPa]
Reduced slenderness	Λ	0.314	[-]
Factor from buckling curve	k	1.000	[-]
Partial safety factor	γ_M	1.15	[-]
Buckling resistance	R_d	282.609	[MPa]
Load factor with imperfection	$R_d/\sigma_{\mathrm{Rep}}$	1.047	Proven
Check	$\sigma_{\mathrm{Rep}}/R_d$	0.955	Proven

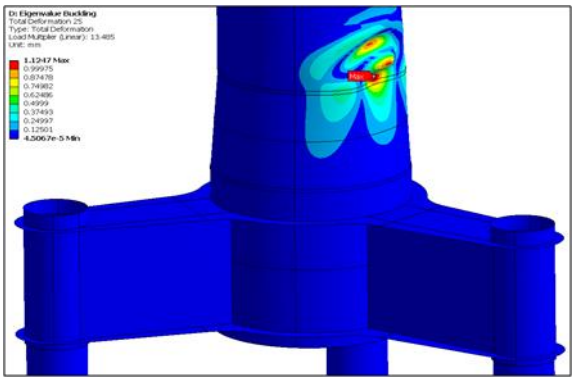

Fig. 23 First local mode at central tubey

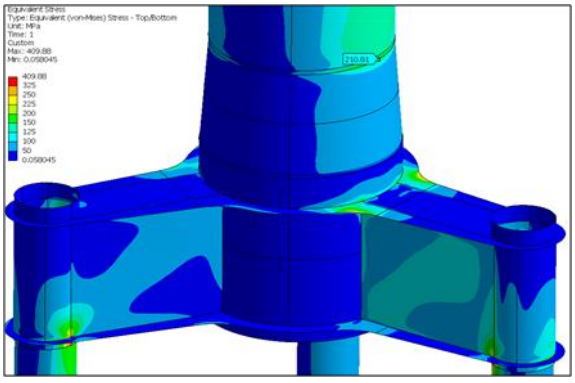

Fig. 24 Local von Mises stresses at central tube

Table 7 Buckling-capability evaluation of central tube

Load case	LC4	Value	Unit
Location of buckling	Ring Stiffener		
Load factor(numerical)	kg	13.485	[-]
Stress at buckling area	σ_{Rep}	211	[MPa]

Critical buckling stress	σ_{ki}	2845.335	[MPa]
Yield strength	f_y	325	[MPa]
Reduced slenderness	Λ	0.338	[-]
Factor from buckling curve	k	1.000	[-]
Partial safety factor	γ_M	1.15	[-]
Buckling resistance	R_d	282.609	[MPa]
Load factor with imperfection	R_d/σ_{Rep}	1.339	Proven
Check	σ_{Rep}/R_d	0.747	Proven

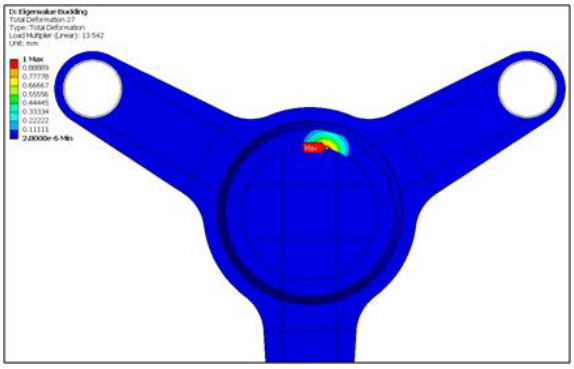

Fig. 25 First local mode at inner ring stiffener

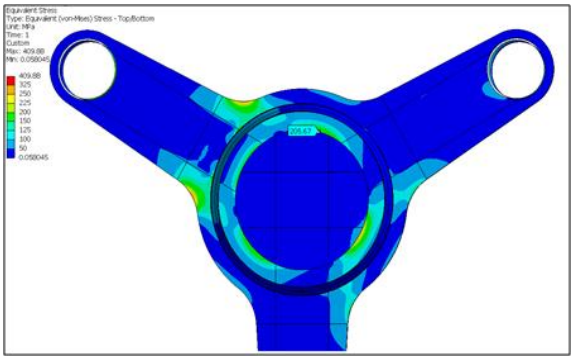

Fig. 26 Local von Mises stresses at inner ring stiffener

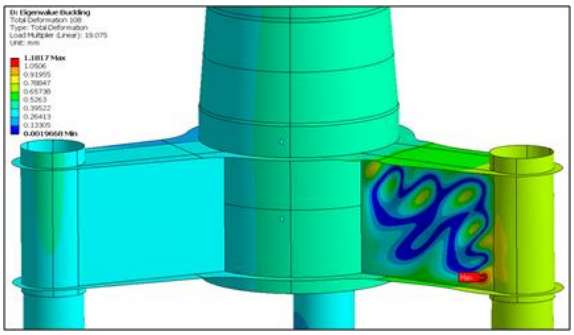

Fig. 27 Local mode at vertical plate at point of maximal von Mises stress

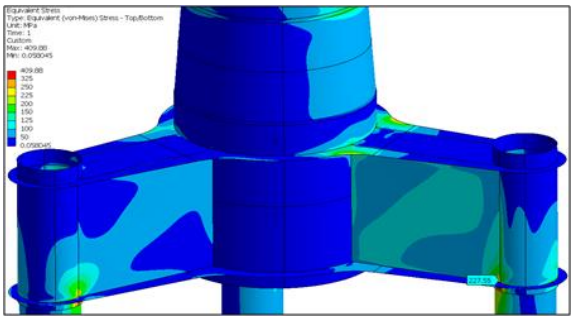

Fig. 28 Local maximal von Mises stresses at vertical plate

Table 8 Buckling-capability evaluation of inner ring stiffener

Load case	LC4	Value	Unit
Location of buckling	Ring Stiffener		
Load factor(numerical)	kg	13.542	[-]
Stress at buckling area	σ_{Rep}	206	[MPa]
Critical buckling stress	σ_{ki}	2789.652	[MPa]
Yield strength	f_y	325	[MPa]
Reduced slenderness	Λ	0.341	[-]
Factor from buckling curve	k	1.000	[-]
Partial safety factor	γ_M	1.15	[-]
Buckling resistance	R_d	282.609	[MPa]
Load factor with imperfection	$R_d/\sigma_{\mathrm{Rep}}$	1.372	Proven
Check	$\sigma_{\mathrm{Rep}}/R_d$	0.747	Proven

therefore obviously lower than the limit of 5% based on DNV-RP-C208. The plastic strain acted locally and was not experienced by the areas surrounding the vertical plates, as shown in Fig. 18. In conclusion, most of the foundation structure was found to exhibit sufficient stress capability according to the ULS evaluation, with the sleeves being the only exception.

3.1.2 ULS verification for the buckling-capability

In this section, the results of the linear buckling analysis (LBA) of the foundation structure are presented. The load considered was that described in Section 2.1.4., with load case 4 being the dominant case. Plots of the important buckling modes and von Mises stresses are presented. The purpose of the analysis was to determine the buckling capacity of the central tube and plated construction parts. The cylindrical sections of the foundation structure were investigated considering the buckling curves given in DIN EN 1993-1-8:2010-12 (Eurocode 3). Because the supporting structure was loaded mostly with bending moments, its buckling mode was a local problem. The plated construction parts were investigated considering the buckling curves given in DNV-RP-C201 with a material sided partial safety factor of $\gamma_{M1} = 1.15$.

The LBA was conducted based on DNV-RP-C201 by investigating the local buckling mode and the local von Mises stresses. First, the buckling modes for each structure part were computed,

Table 9 Buckling-capability evaluation of vertical plate

Load case	LC4	Value	Unit
Location of buckling	Ring Stiffener		
Load factor(numerical)	kg	19.075	[-]
Stress at buckling area	σ_{Rep}	228	[MPa]
Critical buckling stress	σ_{ki}	4349.1	[MPa]
Yield strength	f_y	345	[MPa]
Reduced slenderness	Λ	0.282	[-]
Factor from buckling curve	k	1.000	[-]
Partial safety factor	γ_M	1.15	[-]
Buckling resistance	R_d	300.000	[MPa]
Load factor with imperfection	$R_d/\sigma_{\mathrm{Rep}}$	1.316	Proven
Check	$\sigma_{\mathrm{Rep}}/R_d$	0.760	Proven

as shown in Figs. 19, 21, 23, 25, and 27. The von Mises stresses in the direct vicinity of these locally buckling areas were extracted as shown in Figs. 20, 22, 24, 26, and 28 to determine the critical buckling stresses. The buckling evaluations were performed with the appropriate buckling curves (plates or shells), as shown in Tables 5–9. According to the results, the foundation was able to withstand the ULS loads without losing stability.

3.2 FLS Verification

3.2.1 S-N Curve results

Weld profile stress concentrations arise due to the notches in the weld and are difficult to quantify explicitly using full-scale test results or FE techniques. Consequently, according to DIN EN 1993-1-9 (2010), they should be incorporated into the empirically derived S–N curves. The loads acted as fatigue DELs on the foundation structure of the interface-level tower and were considered in the FE simulations as described in Section 2.1.4. For the fatigue calculations, a cycle number of N = 2.00E8 and a slope of m = 4 were used.

The S–N curves were chosen based on Kolonnenstr without the cut-off limit described by the International Institute of Welding (IIW; 2016). Further modifications were introduced based on DNVGL-RP-C203 (2016) to include offshore-specific conditions. Wall thickness correction factors were used in accordance with Kolonnenstr and DNVGL-RP-C203 (2016). For circumferential welds, the design included a fatigue (FAT) class of 80 MPa with a maximal fabrication misalignment of 10% for 90 MPa and of 5% for 112 MPa (Fig. 30). The maximum weld reinforcements for the fabrication were estimated based on DIN EN 1993-1-9 (2010). However, owing to the missing information in DIN EN 1993-1-9 (2010), the stress concentration factors (SCFs) at the circumferential welds were calculated with equations provided in DNVGL-RP-C203 (2016). Transitions in the wall thickness were adjusted with a slope of 25%. The evaluations of the circumferential weld were conducted considering wall thickness and conical transition as well as the stresses on the smallest section with the maximal SCF value. However, the wall thickness correction factor was calculated for a greater thickness; then, both values were conservatively superpositioned.

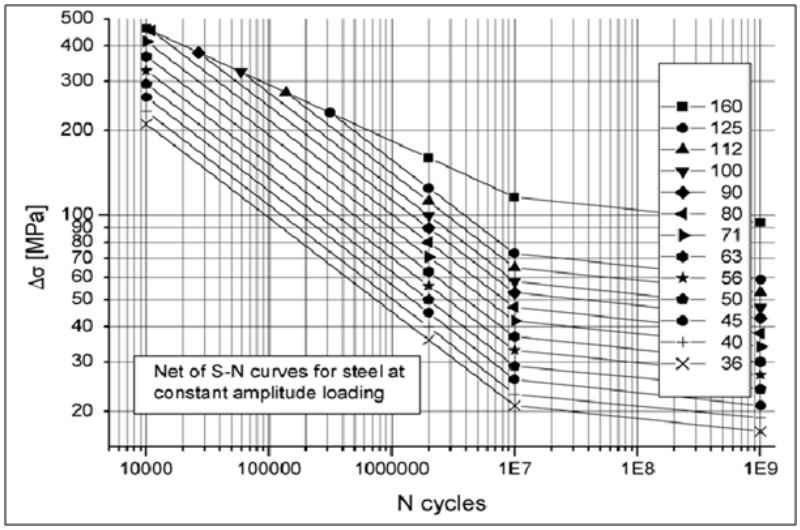

Fig. 29 Fatigue resistance S-N curves for steel, normal stress

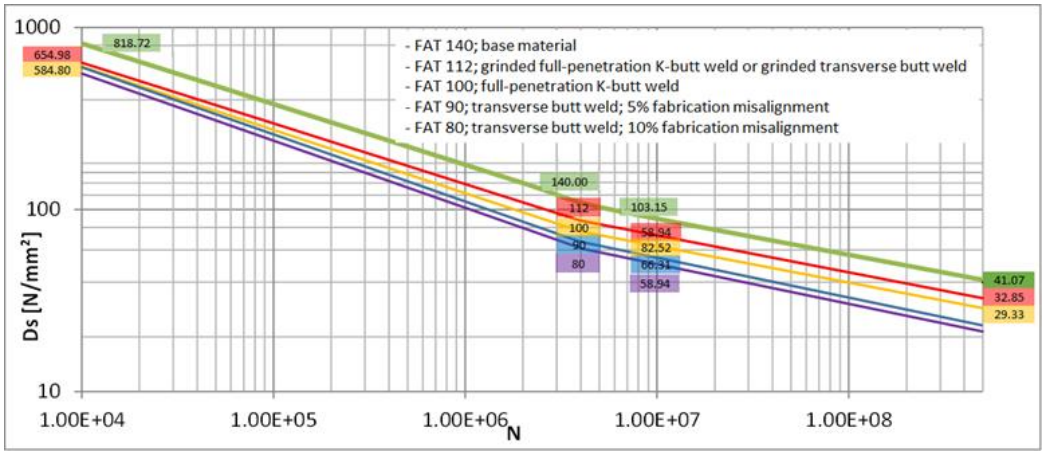

Fig. 30 Result of S-N curve for FAT 80, 90, 100, 112, 140

The evaluation of the circumferential welds was applicable to that of the longitudinal welds (FAT 112). A structural hot-spot stress approach was employed for the welded connections between the central tube and the plated construction parts. FAT classes of 100 and 112 MPa (Fig. 30) were considered for T-joints with full-penetration K-butt welds, along with grinding improvements based on IIW. Any abrupt changes in the cross section or disruptions of the smooth surfaces caused an increase in the stress levels in the vicinity of these regions. Hence, when high stress concentrations were expected at the welded connections, the considered stresses could be extrapolated as described in IIW, according to which welds do not need to be modeled. A stress path normal to the weld that ran from the intersection, where there was maximal stress, to a distance of 1.5 times the base plate thickness t was selected. In the IIW document (Fig. 29), this method is recommended for cases with relatively coarse meshes with higher-order shell elements. The structural hot-spot stress can then be determined as follows:

Table 10 Partial material safety factors for stress ranges for fatigue assessment (Kolonnenstr 2015)

Inspection and accessibility	part of a "nonfail-safe" structure	part of a "fail-safe" structure
Periodic monitoring and maintenance; good accessibility; manufacturing and installation surveillance	1.15	1.0
No periodic monitoring and maintenance possible or poor accessibility (e.g., under water or subsoil)	1.25	1.15
Inspection and accessibility	part of a "nonfail-safe" structure	part of a "fail-safe" structure

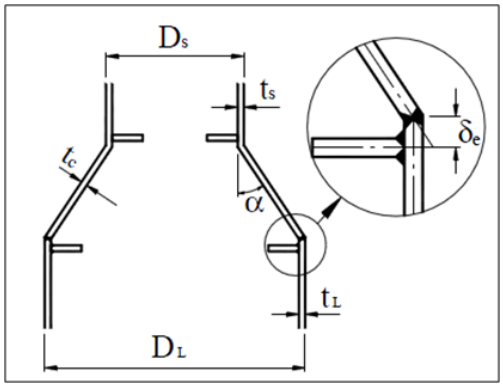

Fig. 31 Cone geometry

$$\sigma_{hs} = 1.5 \cdot \sigma_{0.5t} - 0.50 \cdot \sigma_{1.5t} \text{ (IIW Fatigue Recommendations – Coarse mesh)} \quad (2)$$

To evaluate the base material, a FAT class of 140 MPa was considered (Fig. 30). Based on the material partial safety factors listed in Table 10 (based on DIN EN 1993-1-9 (2010) and Kolonnenstr), a fatigue material safety factor of 1.25 was chosen for a detailed evaluation without periodic inspections. The assessment did not include corrosion allowance.

3.2.2 Result of FLS analysis

In the following, the main calculation steps and results are presented, which provide information on the fatigue damage of the foundation structure. The evaluation results for the circumferential welds in the central tube under Scenarios 1–3 are summarized in Tables 11–13. As an example, the governing SCF values were calculated considering cone transitions based on DNVGL-RP-C203 (2016) for Scenario 1. The SCF values for Scenarios 2 and 3 can be found in Tables 12 and 13.

Regarding the first tubular-cone junction, the SCF at the tubular side dominates, as described in Eqs. (3) and (4):

$$SCF = 1 + \frac{0.6 \cdot t \sqrt{D_j \cdot (t + t_c)}}{t^2} \tan \alpha \quad (3)$$

$$\alpha = \frac{D_L - D_S}{2h_C} \quad (4)$$

Table 11 Evaluation of circumferential welds in central tube for Senario 1

CW	Height Scenario 1	SCF	σ_{ref}	f_t	Damage
-	[m MSL]	-	[MPa]	-	-
1	-2.75	1.00	80	0.758	0.08
2	0.00	1.83	80	0.871	0.36
3	1.75	1.00	80	0.814	0.12
4	3.50	1.88	112	0.902	0.64

Table 12 Evaluation of circumferential welds in central tube for Senario 2

CW	Height Scenario 2	SCF	σ_{ref}	f_t	Damage
-	[m MSL]	-	[MPa]	-	-
1	-7.75	1.00	80	0.758	0.08
2	-5.00	1.36	80	0.758	0.15
3	-3.00	1.00	80	0.814	0.05
4	-1.00	1.00	80	0.814	0.06
5	1.50	1.00	80	0.814	0.06
6	3.50	1.34	90	0.814	0.61

Table 13 Evaluation of circumferential welds in central tube for Senario 3

CW	Height Scenario 3	SCF	σ_{ref}	f_t	Damage
-	[m MSL]	-	[MPa]	-	-
1	-12.75	1.00	80	0.758	0.08
2	-10.00	1.20	80	0.758	0.11
3	-7.00	1.00	80	0.814	0.05
4	-4.00	1.00	80	0.814	0.06
5	-1.50	1.00	80	0.814	0.08
6	1.00	1.00	80	0.814	0.09
7	3.50	1.18	80	0.814	0.58

where D_j is the cylinder diameter at the junction (D_s, D_L), t is the tubular member wall thickness (t_s, t_L), t_c is cone thickness, and α is the slope angle of the cone (see Fig. 31).

Owing to the high stress concentrations at the welded connection between the ring stiffener and the central tube, the stresses were extrapolated in accordance with IIW using a radial stress path normal to the weld. Fig. 32 (a) shows the hot-spot stress with the linear extrapolation. The blue line is the stress distribution as determined by the FEA, while the red line is the stress extrapolation based on IIW. Fig. 32(b) shows the FEA result of minimum principal stress. The estimated hot-spot stress was introduced to estimate the fatigue lifetime (Fig. 33). Owing to the relatively low stress concentrations at the welded connection between the vertical plates and central tube, the maximal principal stress was chosen, as shown in Fig. 34. This connection was evaluated with FAT class 100 MPa and a full-penetration K-butt weld. The evaluation of the

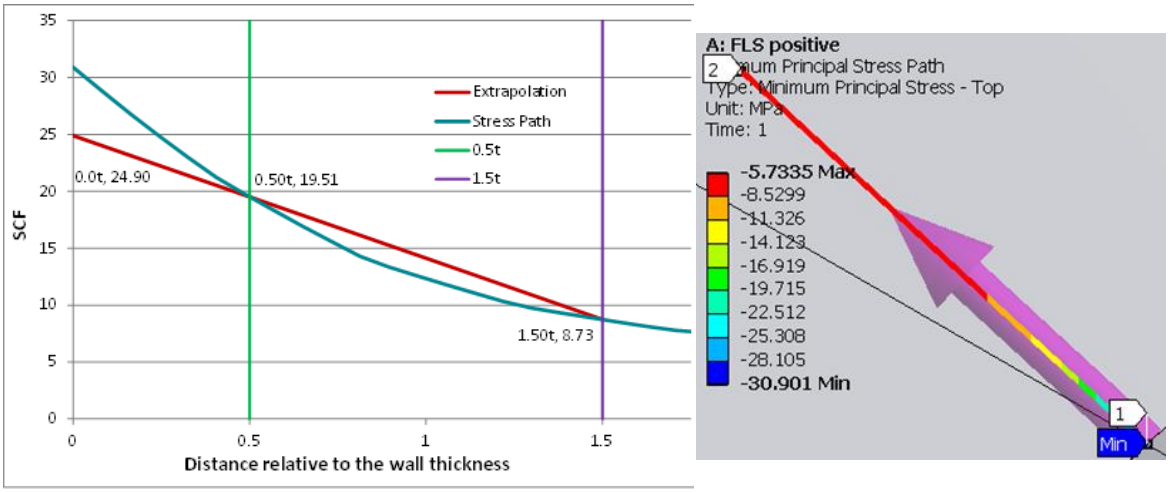

(a) (b)

Fig. 32 (a) Principal stress extrapolation for welded connection of ring stiffener, (b) FEA result

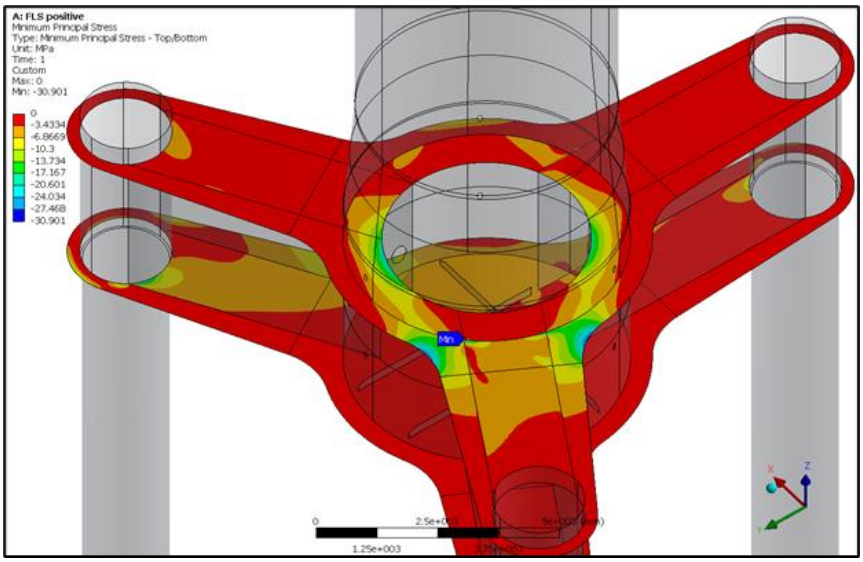

Fig. 33 FLS evaluation of ring stiffener; FAT 112

Table 14 FLS evaluation of ring stiffener; FAT 112

Input Data			f_t	0.90887	[-]
Thickness, t	65	[mm]	n	0.100	[-]
Cycles, N	2.00E+08	[-]	f_w	1.000	[-]
Stress, $\Delta\sigma$	24.90	[MPa]	c	0.000	[-]
N_c	2.00E+06	[-]	γ_M	1.25	[-]
S_{ref}	112	[MPa]	D_1	4.37E-09	[-]
SCF	1.00	[-]	D_{all}	0.8741	[-]

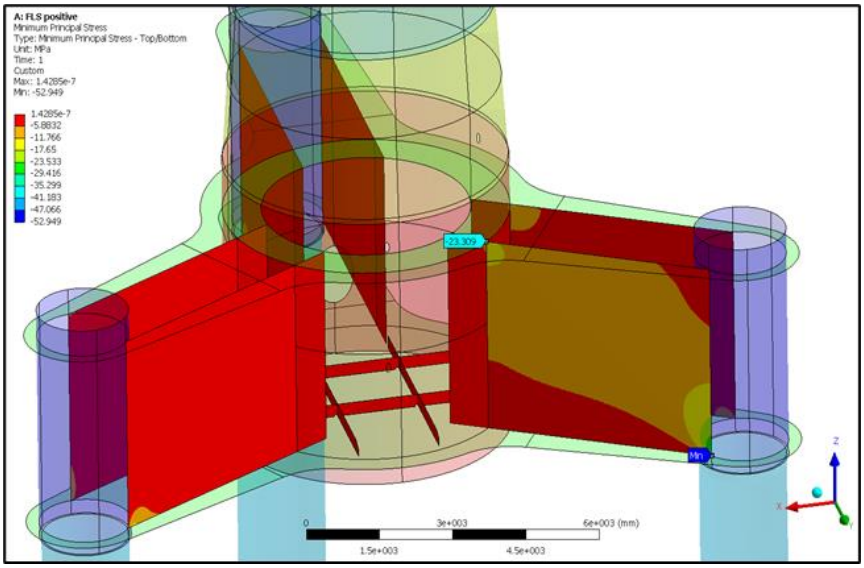

Fig. 34 FLS evaluation of vertical plate; FAT 100

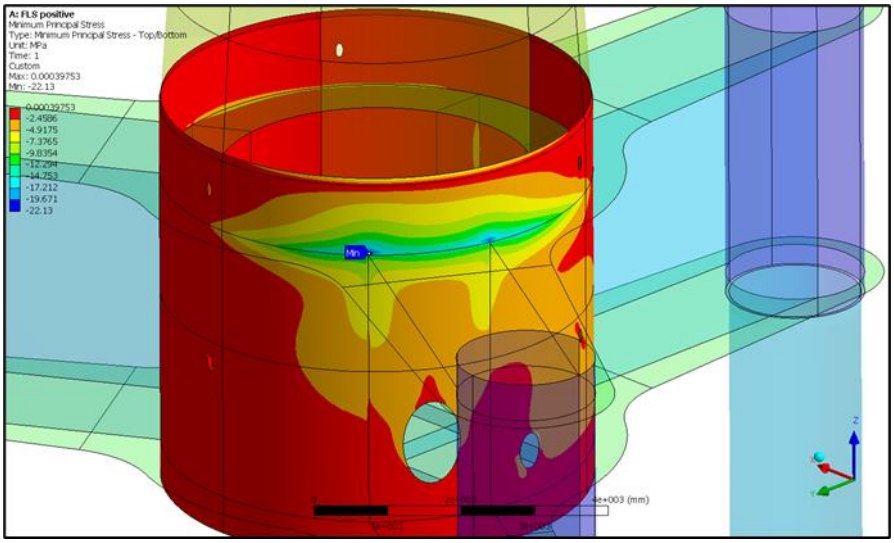

Fig. 35 FLS evaluation of central tube

Table 15 FLS evaluation of vertical plate; FAT 100

Input Data			f_t	0.95409	[-]
Thickness, t	40	[mm]	n	0.100	[-]
Cycles, N	2.00E+08	[-]	f_w	1.000	[-]
Stress, Δσ	23.31	[MPa]	c	0.000	[-]
N_c	2.00E+06	[-]	γ_M	1.25	[-]
S_{ref}	100	[MPa]	D_1	4.35E-09	[-]
SCF	1.00	[-]	D_{all}	0.8699	[-]

Table 16 FLS evaluation of central tube

Input Data			f_t	0.87055	[-]
Thickness, t	100	[mm]	n	0.100	[-]
Cycles, N	2.00E+08	[-]	f_w	1.000	[-]
Stress, Δσ	22.13	[MPa]	c	0.000	[-]
N_c	2.00E+06	[-]	γ_M	1.25	[-]
S_{ref}	112	[MPa]	D_1	3.24E-09	[-]
SCF	1.00	[-]	D_{all}	0.6479	[-]

Table 17 FLS evaluation of ring stiffener

Input Data			f_t	1.00000	[-]
Thickness, t	65	[mm]	n	0.000	[-]
Cycles, N	2.00E+08	[-]	f_w	1.000	[-]
Stress, Δσ	30.28	[MPa]	c	0.000	[-]
N_c	2.00E+06	[-]	γ_M	1.25	[-]
S_{ref}	140	[MPa]	D_1	2.67E-09	[-]
SCF	1.00	[-]	D_{all}	0.5343	[-]

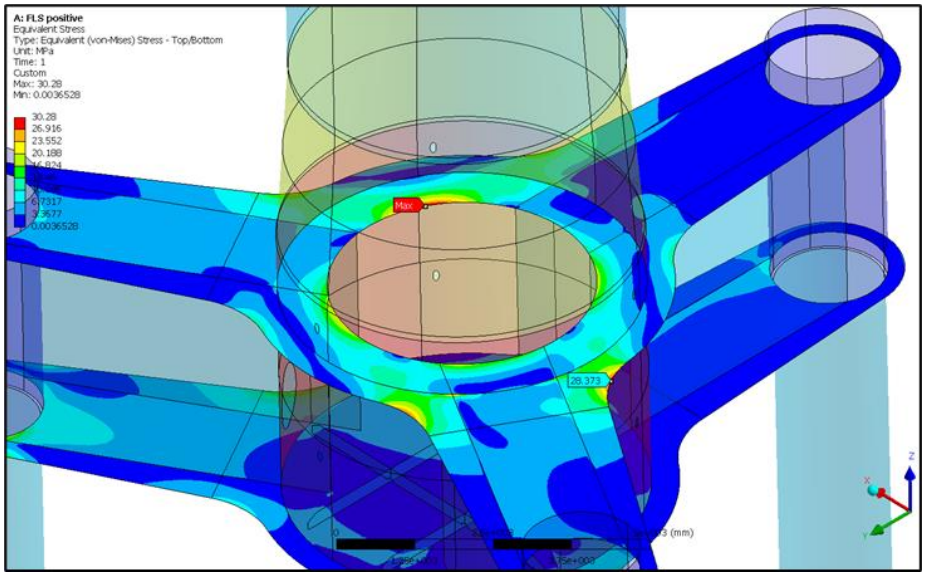

Fig. 36 FLS evaluation of ring stiffener

central tube at the welded connection to the ring stiffener is shown in Fig. 35. The FAT class 112 MPa was also considered for a grinded full-penetration K-butt weld. An FLS evaluation of the welded connections of the vertical plates and ring stiffener to central tube was also conducted. Fig. 36 presents the evaluation of the ring stiffener conducted with FAT class 140 MPa for the base material. The FLS evaluation for the ring stiffener at the free edge is also shown.

In this study, we structurally examined the safety features of the stress concentration of an offshore WTP substructure through the ULS and FLS analysis under three scenarios (Scenarios 1–3). The results of our study revealed that the stress–strain curves for the applied loads differed among Scenarios 1–3.

4. Conclusions

This paper deals with ULS and FLS design, which are the most important factors in substructure design in offshore wind farm development. This paper was written with the hope that research that would be helpful in practice could be conducted by informing and discussing the design process at a practical level to readers.

In conclusion, the results of our ULS evaluation indicate that the foundation structure exhibits a sufficient stress capability except for in the sleeves. The plastic strain at the edges of the connections to the sleeves was found to be irrelevant, as it acted locally and was not experienced by the surrounding areas of the vertical plates. At the same time, the buckling analysis results indicate that the foundation is able withstand ULS loads without losing stability. The behavior of the foundation in Scenarios 1–3 under ULS and FLS was also structurally investigated using an FEM. According to the ULS buckling analysis, the foundation is able to support ULS loads without a risk of instability. The plastic strain was 0.0% in most parts of the structure, although it did occur at higher values locally. Regarding the FLS analysis, the highest stress concentration appeared at the second tubular-cone junction in the central tube in Scenario 1, with an SCF value of 1.88. The results of our stress distribution simulations can be applied to determine the optimal design for MSFs. In future research, we aim to complete an optimal design of the proposed structure and continue to study other substructure types based on our results.

Acknowledgments

This work is the outcome of the SMG offshore wind farm project. The research team collaborated with SMG Offshore Wind Power Ltd., Co., Gigas Engineering Ltd., Co., and the Offshore Power Plant Institute of Jeonbuk National University.

References

Arany, L., Bhattacharya, S., Macdonald, J. and Hogan, S.J. (2016), "Design of monopiles for offshore wind turbines in 10 steps", *Soil Dyn. Earthq. Eng.*, **92**, 126-152, https://doi.org/10.1016/j.soildyn.2016.09.024.

Ashish, C.B. and Selvam, P. (2013), "Static and dynamic analysis of jacket substructure for offshore fixed wind turbines", *Proceedings of the Eighth Asia-Pacific Conference on Wind Engineering*, IIT Madras, India, December.

Bogdán, T.C. (2017), "Numerical modelling of foundations for offshore wind turbines", M.E. Dissertation; University of Aalborg, Aalborg, Denmark.

Brandt, S., Broggi, M., Hafele, J., Gebhardt, C.G., Rolfes, R. and Beer, M. (2017), "Meta-models for fatigue damage estimation of offshore wind turbines jacket substructures", *Procedia Engineering*, **199**, 1158-1163, https://doi.org/10.1016/j.proeng.2017.09.292.

Chen, I.W., Wong, B.L., Lin, Y.H., Chau, S.W. and Huang, H.H. (2016), "Design and analysis of jacket

substructures for offshore wind turbines", *Energies*, **9**(4), 264-282, https://doi.org/10.3390/en9040264.
Chew, K.H., Ng, E.Y.K., Tai, K., Muskulus, M. and Zwick, D. (2014), "Offshore wind turbine jacket substructure: a comparison study between four-legged and three-legged designs", *J. Ocean Wind Energy*, **1**(2), 74-81.
Devaney, L. (2012), "Breaking wave loads and stress analysis of jacket structures supporting offshore wind turbines", M.E. Dissertation; University of Manchester, Manchester, United Kingdom.
DIN EN 10025 (2005), *Hot Rolled Products of Structural Steels - Part 2: Technical delivery conditions for non-alloy structural steels*; Deutsches Institut für Normung, Berlin, Germany.
DIN EN 1993-1-1 (2009), *Eurocode 3: Design of Steel Structures - Part 1-1: General Rules and Rules for Buildings*; Deutsches Institut für Normung, Berlin, Germany.
DIN EN 1993-1-6 (2017), *Eurocode 3: Design of Steel Structures - Part 1-6: Strength and Stability of Shell Structures*; Deutsches Institut für Normung, Berlin, Germany.
DIN EN 1993-1-8 (2009), *Eurocode 3: Design of Steel Structures - Part 1-8: Design of Joints*; Deutsches Institut für Normung, Berlin, Germany.
DIN EN 1993-1-9 (2010), *Eurocode 3: Design of Steel Structures - Part 1-9: Fatigue*, German version EN 1993-1-9:2005 + AC:2009; Deutsches Institut für Normung, Berlin, Germany.
DNV-RP-C201 (2010), *Buckling Strength of Plated Structures*; Det Norske Veritas Germanischer Lloyd, Oslo, Norway.
DNV-RP-C208 (2013), *Determination of Structural Capacity by Non-Linear FE analysis Methods*; Det Norske Veritas Germanischer Lloyd, Oslo, Norway.
DNVGL-OS-C101 (2016), *Design of Offshore Steel Structures: General - LRFD Method*; Det Norske Veritas Germanischer Lloyd, Oslo, Norway.
DNVGL-RP-C203 (2016), *Fatigue Design of Offshore Steel Structures*; Det Norske Veritas Germanischer Lloyd, Oslo, Norway.
DNVGL-RP-C205 (2017), *Environmental Conditions and Environmental Loads*; Det Norske Veritas Germanischer Lloyd, Oslo, Norway.
DNVGL-ST-0126 (2016), *Support Structures for Wind Turbines*; Det Norske Veritas Germanischer Lloyd, Oslo, Norway.
Gerven, F.V. (2011), "Optimising the design of a steel substructure for offshore wind turbines in deeper waters", M.E. Dissertation; Delft University of Technology, Delft, Netherlands.
Gholipour, M. and Mazloom, M. (2018), "Seismic response analysis of mega-scale buckling-restrained bracing systems in tall buildings", *Adv. Comput. Des.*, **3**(1), 17-34, https://doi.org/10.12989/acd.2018.3.1.017.
Hobbacher, A. (2016), *International Institute of Welding (IIW): Recommendations for Fatigue Design of Welded Joints and Components*, Springer, Berlin, Germany.
Kelma, S. and Schaumann, P. (2015), "Probabilistic fatigue analysis of jacket support structures for offshore wind turbines exemplified on tubular joints", *Energy Procedia*, **80**, 151-158, https://doi.org/10.15488/782.
Kolonnenstr, G.B. (2015), *Guideline for Wind Turbines Effect and Proof of Stability for Tower and Foundation*, Texts of the German Institute for Civil Engineering Series B, **8**.
Maier, S. (2015), "Feasibility of offshore wind substructures in arctic environments", M.E. Dissertation; Delft University of Technology, Delft, Netherlands.
Mo, R., Kang, H., Li, M. and Zhao, X. (2017), "Seismic fragility analysis of monopile offshore wind turbines under different operational conditions", *Energies*, **10**(7), 1037-1059, https://doi.org/10.3390/en10071037.
Svensson, H. (2010), "Design of foundations for wind turbines", M.E. Dissertation; University of Lund, Lund, Sweden.
Ushio, Y., Saruwatari, T. and Nagano, Y. (2019), "Elastoplastic FEM analysis of earthquake response for the field-bolt joints of a tower-crane mast", *Adv. Comput. Des.*, **4**(1), 53-72, http://doi.org/10.12989/acd.2019.4.1.053.
Yeter, B., Garbatov, Y. and Soares, C.G. (2016), "Evaluation of fatigue damage model predictions for fixed

offshore wind turbine support structures", *Int. J. Fatigue*, **87**, 71-80, https://doi.org/10.1016/j.ijfatigue.2016.01.007.
Zaaijer, M.B. (2002), "Foundation models for the dynamic response of offshore wind turbines", *Proceedings of the Marine Renewable Energy Conference (MAREC)*, Newcastle.

CC